



HAL
open science

Ion pair supramolecular structure identified by ATR-FTIR spectroscopy and simulations in explicit solvent

Jeremy Donon, Sana Habka, Thibaut Very, Florence D J Charnay-Pouget,
Michel Mons, David J Aitken, Valérie Brenner, Eric Gloaguen

► **To cite this version:**

Jeremy Donon, Sana Habka, Thibaut Very, Florence D J Charnay-Pouget, Michel Mons, et al.. Ion pair supramolecular structure identified by ATR-FTIR spectroscopy and simulations in explicit solvent. *ChemPhysChem*, 2021, 22 (23), pp.2442-2455. 10.1002/cphc.202100565 . hal-03783652

HAL Id: hal-03783652

<https://hal.science/hal-03783652v1>

Submitted on 22 Sep 2022

HAL is a multi-disciplinary open access archive for the deposit and dissemination of scientific research documents, whether they are published or not. The documents may come from teaching and research institutions in France or abroad, or from public or private research centers.

L'archive ouverte pluridisciplinaire **HAL**, est destinée au dépôt et à la diffusion de documents scientifiques de niveau recherche, publiés ou non, émanant des établissements d'enseignement et de recherche français ou étrangers, des laboratoires publics ou privés.

Ion pair supramolecular structure identified by ATR-FTIR spectroscopy and simulations in explicit solvent

Jeremy Donon,^{a,*} Sana Habka,^a Thibaut Very,^{a,‡} Florence Charnay-Pouget,^{b,§} Michel Mons,^a
David J. Aitken,^b Valérie Brenner,^a Eric Gloaguen^{a,*}

-
- [a] Dr. J. Donon, Dr. S. Habka, Dr. T. Very, Dr. M. Mons, Dr. V. Brenner, Dr. E. Gloaguen
LIDYL, CEA, CNRS, Université Paris Saclay
CEA Saclay, Bât 522, 91191 Gif-sur-Yvette, France
E-mails: jeremy.donon@outlook.fr; eric.gloaguen@cea.fr
- [b] F. Charnay-Pouget, Pr. D. J. Aitken
ICMMO, CNRS, Université Paris Sud, Université Paris Saclay, UMR 8182
Bât. 420, 15 rue Georges Clémenceau, 91405 Orsay cedex, France
- [‡] Dr. T. Very
Present address
IDRIS-CNRS
Campus Universitaire d'Orsay, BP 167, 91403 Orsay cedex, France
- [§] F. Charnay-Pouget
Present address
Université Clermont Auvergne, CNRS, SIGMA Clermont, ICCF
F-63000 Clermont-Ferrand, France

Abstract

The present work uses ATR-FTIR spectroscopy assisted by simulations in explicit solvent and frequency calculations to investigate the supramolecular structure of carboxylate alkali-metal ion pairs in aqueous solutions. ATR-FTIR spectra in the 0.25 – 4.0 M concentration range displayed cation-specific behaviors, which enabled the measurement of the appearance concentration thresholds of contact ion pairs between 1.9 and 2.6 M depending on the cation. Conformational explorations performed using a non-local optimization method associated to a polarizable force-field (AMOEBa), followed by high quantum chemistry level (RI-B97-D3/dhf-TZVPP) optimizations, mode-dependent scaled harmonic frequency calculations and **electron density analyses**, were used to identify the main supramolecular structures contributing to the experimental spectra. A thorough analysis enables us to reveal the mechanisms responsible for the spectroscopic sensitivity of the carboxylate group and the respective role played by the cation and the water molecules, highlighting the necessity of combining advanced experimental and theoretical techniques to provide a fair and accurate description of ion pairing.

Introduction

Pairing between a cation and an anion occurs frequently in environments that are rich in ions, forming supramolecular objects, namely ion pairs. Their formation, particularly in aqueous solutions,^[1] is of paramount importance in a large variety of natural processes or engineered systems, ranging from simple chemical reactions,^[2-4] electron transfer,^[5-7] to stabilization and folding of macromolecular structures like proteins^[8-10] or DNA.^[11, 12] Mastering ion-pairing is, in turn, necessary to model cross-cutting applications in biology, atmospheric chemistry, geochemistry and electrochemistry.^[13-15] One of the most nagging question relates on the type of ion pairs in equilibrium with free ions (FIs). Contact ion pairs (CIPs) and solvent-shared ion pairs (SIPs) constitute such archetypical supramolecular structures resulting from the interactions between ions and solvent molecules.^[15] The ion pair type distribution depends on many parameters, especially the nature and concentration of the ions and the type of solvent. However, the co-existence of different types of ion pairs and their elusive nature in solution make them difficult to characterize.

Despite countless experimental and theoretical studies, the knowledge of the bonding properties of ions of opposite charges in aqueous solution is a longstanding fundamental issue.^[15] To date, various advanced techniques have been used to examine ion pairs in different environments, such as conductometry,^[16] potentiometry,^[17-19] nuclear magnetic resonance (NMR),^[20-24] ultrasonic relaxation,^[25, 26] dielectric relaxation,^[14, 27-29] X-ray scattering and absorption,^[30-32] UV-visible spectroscopy,^[33, 34] and near infrared spectroscopy,^[9, 35-41] but they are largely considered to probe only indirectly ion association, and most of them are unevenly sensitive to the different types of pairings.^[15, 34] Meanwhile, theoretical approaches often struggled to provide an accurate picture of ion pairing.^[42-49] This ultimate goal can interestingly be achieved in microsolvation studies,^[38, 50-52] but unfortunately only for clusters with a limited number of solvent molecules. Overall, it is difficult to access a reliable microscopic picture of ion pairing in solution, where the neighboring solvent molecules that stabilize and shape the ion pair can be distinguished from the others. Indeed, in aqueous solutions, the interplay between all intermolecular forces involving the ions and the water molecules of the first solvation shell already induces highly complex supramolecular organizations that are difficult to identify or characterize. The molecular organization of electrolytic solution depends strongly on the specific nature of the ions,^[53] and

their impact on the bulk is a long running debate.^[54-57] The issue of ion-pairing thus remains too often qualitatively addressed under the guidance of general principles and empirical rationalizations such as that provided by Collins based on the ion charge density, low or high for chaotrope or kosmotrope ions respectively.^[13]

Being simple models for ion pairing investigations, aqueous solutions of alkali-metal acetate have received special attention^[31, 32, 37, 48, 58] due to the significance of carboxylate (CO_2^-) pairing at the solvent-protein interface.^[59-61] The symmetric stretching of the CO_2^- group ($\sigma(\text{CO}_2^-)^{\text{sym}}$, $\sim 1350\text{-}1500\text{ cm}^{-1}$) and the asymmetric stretching ($\sigma(\text{CO}_2^-)^{\text{anti}}$, $\sim 1500\text{-}1600\text{ cm}^{-1}$) are sensitive to the way the group is bound to alkali cations,^[62, 63] making vibrational spectroscopy appropriate to monitor ion pair formation. Recently, we reported an original approach where accurate gas phase spectroscopic data were used to refine high level quantum chemistry frequency calculations of ion pairs in solution, resulting in an unprecedented interpretation of ATR-FTIR spectra of sodium acetate solutions in terms of ion pair formation.^[64] Going beyond the description of an ion pairing surrounded by a too simple solvent model (*i.e.* continuum or a few explicit water molecules),^[65] frequency calculations were performed at the DFT-D level on systems solvated by at least two shells of explicit water molecules plus a solvent continuum model. In the present work, we apply the same combined experimental and theoretical approach to the alkali-metal cation series from Li^+ to Cs^+ in order to document how ion pairing is sensitive to the nature of the cation. In addition, Natural Bond Orbital calculations were carried out in order to rationalize the electronic response of the carboxylate probe to its environment and relate it to vibrational frequencies. This article is organized as follows. After briefly reviewing the experimental and computational methods, ATR-FTIR spectra of electrolyte solutions at different concentrations are reported for the series (AcO^- , M^+), where $\text{M} = \text{Li}, \text{Na}, \text{K}$ and Cs ; then, the structural and spectroscopic properties of ion pairs resulting from the simulations in explicit solvent are presented and discussed; finally, ATR-FTIR spectra are interpreted by comparison with the theoretical results.

Results and discussion

ATR-FTIR Studies

ATR-FTIR spectra of sodium acetate solutions and quantum-chemistry computations recently showed that the stretching modes of carboxylate are sensitive to ion pairing, allowing the detection and identification of specific types of solvent-shared and contact ion pairs.^[64] Following the same approach, ATR-FTIR spectra of lithium, potassium, rubidium and cesium acetate solutions of increasing concentrations were recorded from 0.25 to 4 M (Fig. S4). In these experiments, not only the fraction of paired ions is expected to increase relatively to that of the free ions, but the distributions between the different types of ion pairs, SIPs and CIPs, can also be modulated.

All spectra display a first intense transition in the 1350-1460 cm^{-1} range attributed to the CO_2^- symmetric stretching mode, although a mixing with the CC stretch is known to occur,^[51] and a second one in the 1460-1600 cm^{-1} range corresponding to the CO_2^- antisymmetric stretching mode. As the concentration is increased, their peak position (Fig. 1) and their full width at half maxima (FWHM) display variations similar to that previously reported for sodium acetate.^[64]

In all systems, the FWHM of the $(\text{CO}_2^-)^{\text{sym}}$ and $(\text{CO}_2^-)^{\text{anti}}$ transitions are respectively 39 ± 2 and $60 \pm 3 \text{ cm}^{-1}$ at the lowest concentration, far beyond the intrinsic width of vibrational transitions ($\sim 10 \text{ cm}^{-1}$ for each CO_2^- stretching bands in the gas phase).^[64] At low concentration, this significant width is ascribed to temperature and solvent broadening. However, the FWHM still increases with the concentration (up to ~ 12 and $\sim 20 \text{ cm}^{-1}$ FWHM increase for the symmetric and antisymmetric modes, respectively) revealing an increasing diversity of structures in which the CO_2^- group is engaged, in agreement with ion pair formation. The spectral shifts (Fig. 1) resulting from the increase in concentration will thus be interpreted as resulting from acetate population transfers from free to paired ions, and between the different types of ion pairs themselves.

For all systems, both CO_2^- stretching bands redshift when the ion concentration increases (Fig. 1). This shift is also reflected in the second-derivative spectra shown in Fig. S4. Qualitatively, these spectral shifts are very similar along the cation series: (i) for each mode and each cation, transitions first shift linearly at low concentration; (ii) then, a change of slope occurs typically

between 1.9 and 2.6 M; (iii) transitions finally shift again linearly at high concentration. The linear fits of the low concentration region lead to very similar extrapolations at infinite dilution (0 M) whatever the cation considered, *i.e.* 1415.1 ± 0.3 and 1551.5 ± 0.3 cm^{-1} , for $\sigma^0(\text{CO}_2^-)^{\text{sym}}$ and $\sigma^0(\text{CO}_2^-)^{\text{anti}}$ respectively. These values, common to the five systems investigated, are thus assigned to that of free acetate ions and highlight the accuracy of the measurements and the consistency of the five datasets.

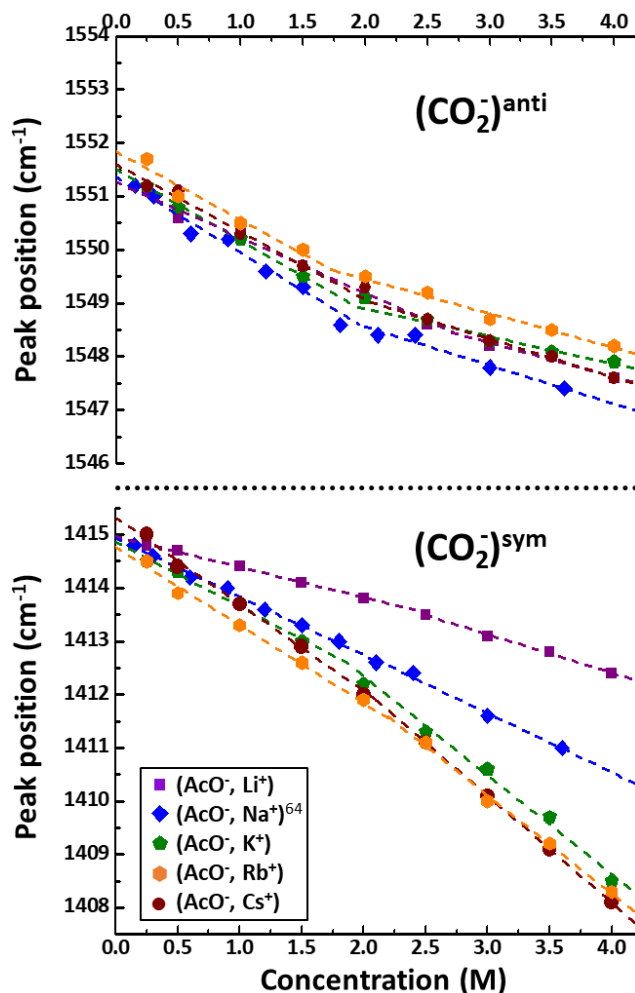


Fig. 1 Peak position of the $(\text{CO}_2^-)^{\text{sym}}$ (down) and $(\text{CO}_2^-)^{\text{anti}}$ (top) transitions of ATR-FTIR spectra presented in Fig. S4, as a function of concentration. Dotted lines are the best linear fit passing through low and high concentration subsets.

Focusing our analysis on the low concentration region, one observes that spectral shifts of the $(\text{CO}_2^-)^{\text{sym}}$ transitions depend on the nature of the cation, especially for Li^+ and Na^+ , which is consistent with ion pair formation. Several considerations lead us to assign these ion pairs to SIPs. First, the extrapolation at infinite dilution of the spectral shifts suggests that the latter result

from a process directly involving the free ions, which is consistent with the idea that SIP formation from free ions is the first step of ion pairing. Second, the concentration range considered (~ 0.15 - 2.0 M) is consistent with SIP formation according to molecular dynamic simulations, which found that CIP concentration is negligible at 1 M.^[48] Indeed, when concentration increases, the number of water molecules available per (AcO^- , M^+) entity is always sufficient to form SIPs, although, at ~ 2 M, this number gets actually close to the minimum number needed to complete a first solvation shell around each ion (*i.e.* 22-25 comprising 16 water molecules for acetate,^[66] and ~ 4 to 7 for the alkali cation depending on its nature^[66, 67]). CIPs are thus expected to be present in this ~ 2 M concentration range where Fig. 1 shows a change of slope, which may thus be assigned to a CIP appearance threshold. In order to push further the interpretation of these spectra and identify the type of supramolecular structures responsible for these shifts, simulations at an advanced level of theory were conducted as explained below.

Simulations and DFT Computations

Explorations of the conformational landscape of $(\text{AcO}^-, \text{M}^+) \cdot (\text{H}_2\text{O})_N$ clusters were performed for the four cations studied here ($\text{M} = \text{Li}, \text{K}, \text{Rb}$ and Cs), following the same approach as that used for $\text{M} = \text{Na}$ ^[64]. The generated structures (around 50,000 for each cation) are reported on a map (Fig. 2 and S5) showing the relative position of the ions according to two parameters: the $\text{O}_{\text{carboxylate}}-\text{O} \cdots \text{M}^+$ dihedral angle, noted θ , and the unsigned distance difference $|\Delta d|$ between the cation and both oxygen atoms of the carboxylate group. The CIP and SIP sets (red and blue) are distinguished after considering the cation-anion distance distributions, which display a sharp peak at short distances corresponding to CIPs, and a broad peak at larger distances mainly corresponding to SIPs. Then, the minimum between these two peaks is used as a criterion to sort CIPs and SIPs as described in the electronic supplementary information (Fig. S3). The dihedral angle θ varies from 0° to 180° and $|\Delta d|$ from 0 to 225 pm, which shows the wide diversity of the structures obtained. Explorations were thus considered sufficiently exhaustive to provide a good characterization of the conformational landscape.

A first qualitative comparison of the maps of Fig. S5 allows us to sort cations in two categories: Li^+ and Na^+ on one side, K^+ , Rb^+ and Cs^+ on the other side. Firstly, these two sets differ in the

ion pair type distributions: the SIP/CIP ratio is typically twice larger for the former set than for the latter. Secondly, $(\text{AcO}^-, \text{Li}^+)$ and $(\text{AcO}^-, \text{Na}^+)$ CIP structures are much less spread on the map than for the other cations. Additional differences can be revealed by a more thorough analysis detailed below.

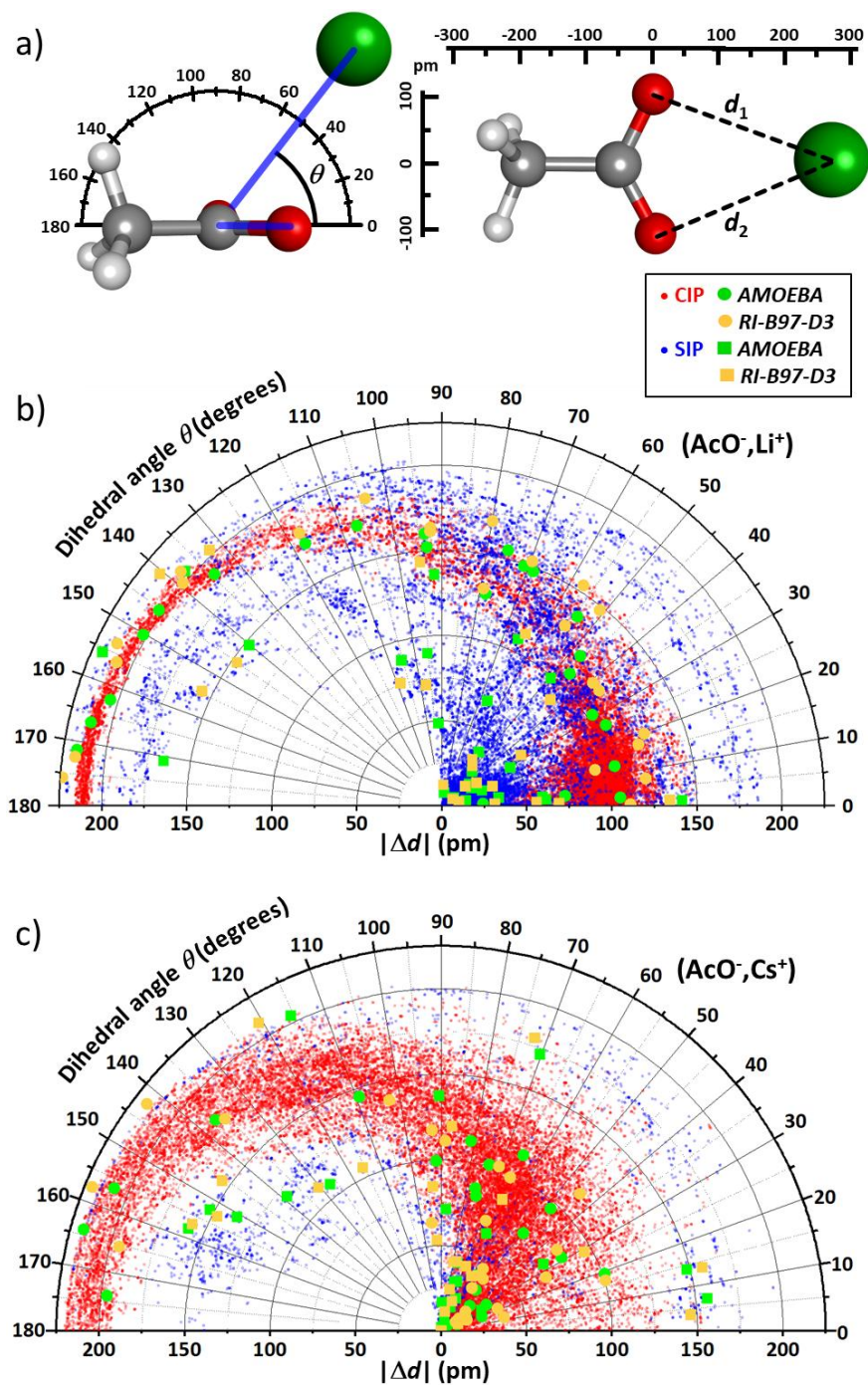


Fig. 2 Maps presenting the structures resulting from the conformational explorations of $(\text{AcO}^-, \text{M}^+) \cdot (\text{H}_2\text{O})_N$ clusters for $\text{M} = \text{Li}$ (b) and Cs (c). CIP (red) and SIP (blue) structures are reported as a function of the $\text{O}-\text{C}_{\text{carboxylate}}-\text{O} \cdots \text{M}^+$ dihedral angle θ and the unsigned difference $|\Delta d|$ between the two distances d_1 and d_2 (a). Sampled AMOEBA structures are identified by green symbols (circles for CIPs and squares for SIPs), and the corresponding RI-B97-D3/dhf-TZVPP optimized $(\text{AcO}^-, \text{M}^+) \cdot (\text{H}_2\text{O})_n$ structures are represented by orange symbols (see Fig. S5 for enlarged pictures and results for the other cations).

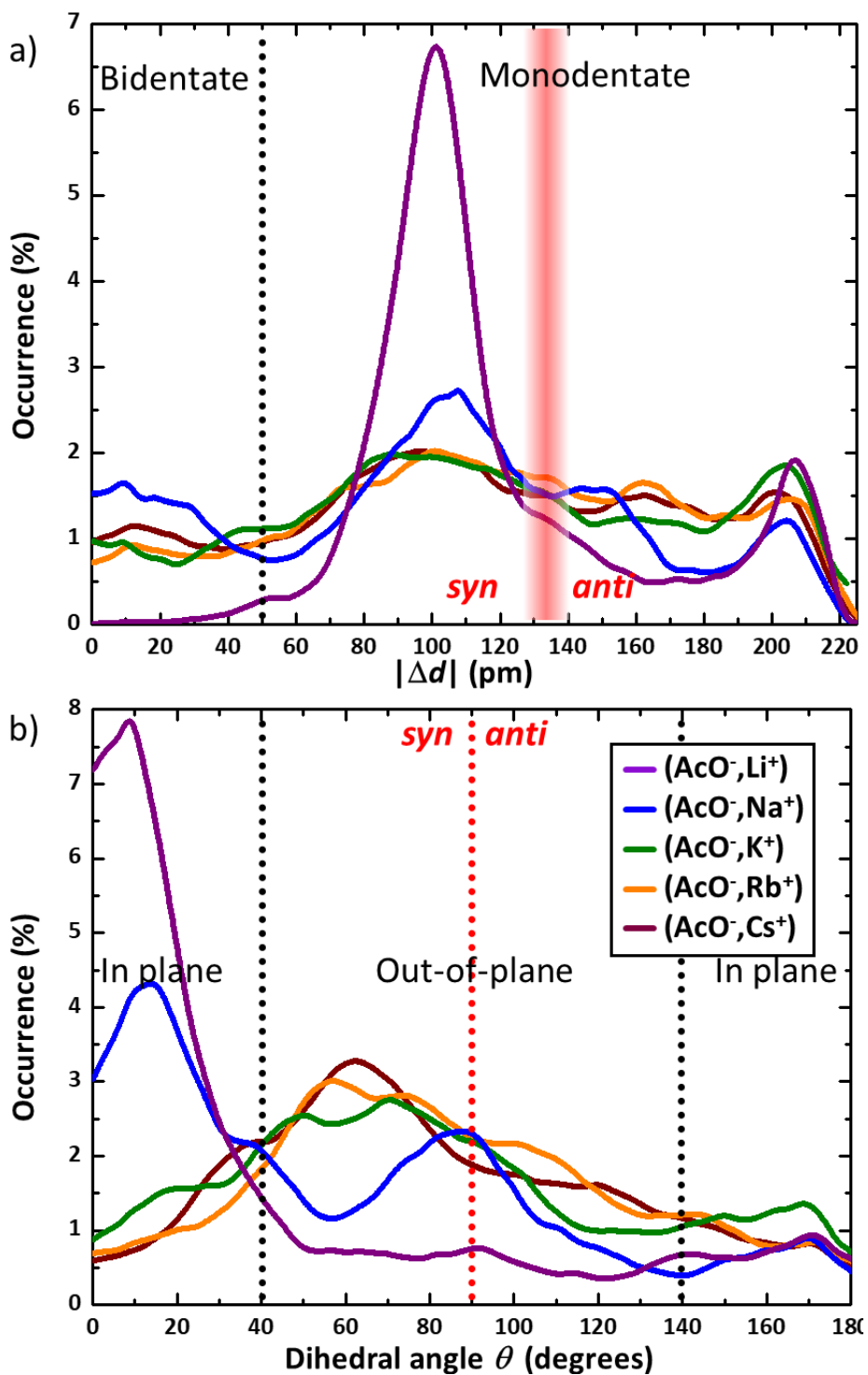


Fig. 3 Smoothed distributions of $|\Delta d|$ (a), and θ (b) (see Fig. 1a for definitions) in CIP structures found by simulations using AMOEBA on $(\text{AcO}^-, \text{M}^+) \cdot (\text{H}_2\text{O})_N$ clusters for $\text{M} = \text{Li}, \text{Na}, \text{K}, \text{Rb}, \text{Cs}$. Occurrences are given for 3 pm and 3° bin widths respectively. Vertical lines delimit $|\Delta d|$ and θ ranges corresponding to the different archetypal ion pair structures discussed in the text, *i.e.* bidentate, *syn*- or *anti*-monodentate, and in plane or out-of-plane pairing geometries.

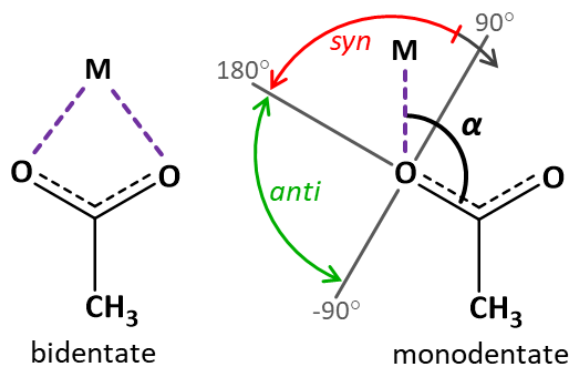


Fig. 4 Binding geometries and naming conventions for metal ion carboxylate adapted from Carrell *et al.*,^[68] where α is the $C_{\text{carboxylate}}\text{-O}\cdots\text{M}^+$ bond angle projected onto the carboxylate plane. Note that *syn*-monodentate type of binding lies in the $\alpha=[100^\circ, 180^\circ]$ range, *anti*-monodentate lies in the $[-180^\circ, -90^\circ]$ range, and bidentate binding lies in the $[80^\circ, 100^\circ]$ range.

In order to assign IR spectra, a deeper structural analysis going beyond the too simplistic categories CIPs and SIPs is needed. Considering that the IR signature of the carboxylate group should be primarily governed by the cation position relative to it, we first focused our analysis on the cation-anion interaction.

First, CIP structures were analysed based on $|\Delta d|$ distributions (Fig. 3a). Different $|\Delta d|$ ranges can be distinguished: $[0\text{-}50\text{ pm}]$, for bidentate, and $[50\text{-}225\text{ pm}]$ for monodentate species. Considering further the angle α (Fig. 4), one observes that *syn*-monodentate species typically lie in the $|\Delta d| = [50\text{-}135\text{ pm}]$ region, and *anti*-monodentate in the $[135\text{-}225\text{ pm}]$ range (see also Fig. S6). Figure 3a shows that the distribution of structures between these categories depends on the nature of the cation. In the case of Li^+ , the majority of structures are *syn*-monodentates (peak at $|\Delta d| \sim 100\text{ pm}$). A small fraction of *anti*-monodentates species is also observed at $\sim 210\text{ pm}$, whereas bidentate species ($< 50\text{ pm}$) are remarkably negligible in comparison. For Na^+ , *syn*-monodentate species (peak at $\sim 110\text{ pm}$) still dominate over *anti*-monodentates species ($\sim 150\text{ pm}$ and $\sim 210\text{ pm}$), but the presence of bidentate species can be clearly seen ($\sim 15\text{ pm}$). The distributions obtained with K^+ , Rb^+ and Cs^+ are very similar, spread over a wide range of $|\Delta d|$ from 0 to 230 pm, with a domination of monodentate species, but where it is more difficult to differentiate each category compared to Li^+ and Na^+ .

The distribution of CIP structures along the dihedral angle θ is shown on Figure 3b. The position of the cation relative to the carboxylate plane also depends on the nature of the cation,

particularly in the case of Li^+ and Na^+ . In these cases, the cation is mainly located in the carboxylate plane ($\theta < 40^\circ$). For Na^+ , two other angle ranges are frequently observed, the first around 90° , corresponds to monodentate conformations where the cation is out of the carboxylate plane, and the second around 170° , can be associated to monodentate *anti*-conformations where the cation is in the carboxylate plane. Note that $\theta = 90^\circ$ marks the limit between *anti*- and *syn*-monodentate types. In contrast, systems containing cations of larger ionic radii, *i.e.* K^+ , Rb^+ and Cs^+ (ionic radii of Li^+ , Na^+ , K^+ , Rb^+ and Cs^+ are 76, 102, 138, 152 and 167 pm respectively)^[69] have a relatively similar distribution profile, dominated by a very broad peak centred around $\theta = 65^\circ$, which indicates that these cations are mainly located out of the carboxylate plane, but their angular position is less peaked than those of Li^+ and Na^+ . The different θ and $|\Delta d|$ distribution behavior of the alkali-metals illustrates the relatively higher capability of small cations to form highly-organized supramolecular structures in aqueous solutions, echoing the kosmotrope vs. chaotrope ion classification.^[13]

In the case of SIPs, a larger diversity of structures is observed (Fig. 2 and S5). In addition, no cation-specific pattern emerges from these maps, illustrating a poor directionality of the cation-anion interaction in SIPs whatever the cation considered.

The structures selected for geometry optimization and frequency calculations were chosen in different regions of the maps of Fig. 2 and S5 in order to account for the diversity of the cation-anion arrangements found in the exploration. The carboxylate group being used as a probe of its supramolecular environment, candidate structures were also chosen according to the arrangement of the first coordination shell of the carboxylate group in order to reflect the variety of environments around the probe and also avoid duplicate calculations. In practice, a first sampling was carried out by selecting low-energy structures in each significantly populated area of the maps of Fig. 2 and S5, then an additional sampling was conducted to complete the sets of structures to account for the various arrangements of the first solvent shell around the carboxylate group, resulting in the green set of structures on Fig. 2 and S5. RI-B97-D3 optimized structures (orange sets on Fig. 2 and S5) were found to lie in the same area of the map as the initial AMOEBA structures (green sets), illustrating that no important geometric changes (*e.g.* CIP-SIP isomerization, change of cation-anion interaction, H-bond network rearrangement) occurred during optimization, thus justifying the relevance of the first step of our theoretical approach.

Theoretical spectral signatures

The vibrational signature of the carboxylate group depends primarily on its immediate environment, *i.e.* the first shell containing the solvent molecules and the cation in the case of CIPs. As we noticed previously for free acetate ions,^[64] numerous arrangement of the first solvation shell exist around the CO_2^- group. For the ion pairs studied here, the number of water molecules H-bound to the oxygen atoms of the CO_2^- group varies between 5 and 6 for SIPs, and decreases to 4-5 for CIPs, where the alkali cation takes the place of one water molecule of the first solvation shell of the carboxylate, keeping a coordination number similar to that of the free carboxylate anion (found to be 6 in ref.^[66] and between 5 and 6 in this study as shown on Fig. 5). Regarding cations, their coordination number (CN) is found equivalent to that of the free cations in aqueous solution^[67] for Li (CN = 4), Na (CN = 5) and K (CN = 6), and decreased by one unity down to 7 for Rb and Cs (Table S3).

For IR analysis purposes, CIP and SIP structures were thus sorted into eight categories according to the coordination types of the carboxylate group, *i.e.* the number and nature of ligands (water molecules or metal cation) on each oxygen atom of the CO_2^- group, as well as the number of water molecules bridging the latter and the cation for SIPs. One structure of each category is depicted in Fig. 5, the other surrounding water molecules of the $(\text{AcO}^-, \text{M}^+) \cdot (\text{H}_2\text{O})_n$ clusters being not shown for clarity purposes. Structures were named using the nomenclature defined for AcO^- and $(\text{AcO}^-, \text{Na}^+)$ in our previous article.^[64] The sets $(n|m)$ correspond to free acetate ions where the coordination number of oxygen atoms is n and m . The sets $(\underline{n}|m)$ correspond to CIP structures, where the underlined label indicates that the cation is among the n ligands (monodentate bonding). In addition, the label $(n[\underline{s}]m)$ is used to specify that s ligands bridge both oxygen atoms and that the cation is among them (bidentate chelating bond); for SIPs, ${}^a(n|m)^b$ is used for structures where a of the n (resp. b of the m) water molecules belong also to the first solvation shell of the cation. As already mentioned, no bidentate structure was found in the case of $(\text{AcO}^-, \text{Li}^+)$. However, a specific category, $(\underline{2}|2)$, was identified but was further neglected due to its weak occurrence (Table S4).

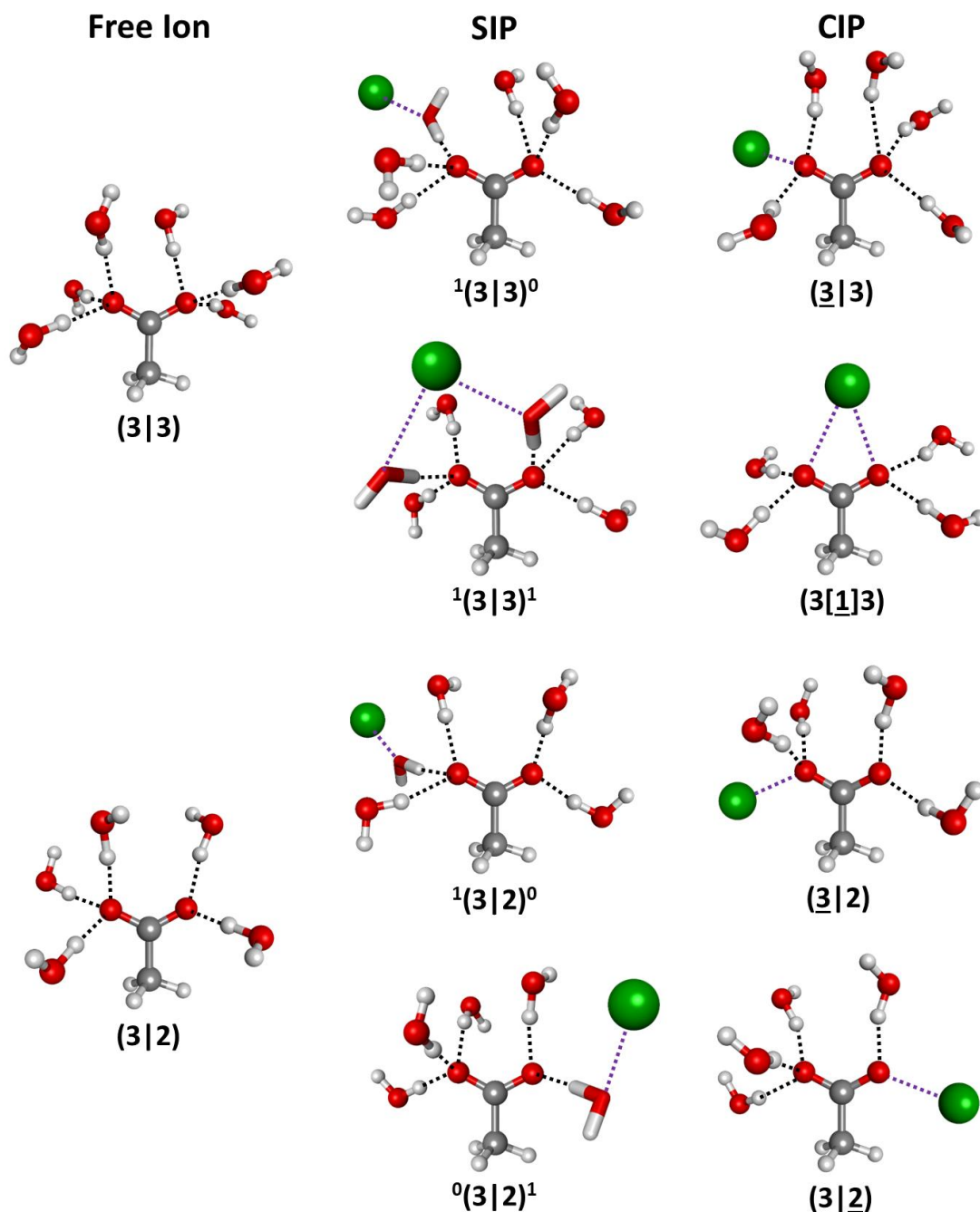


Fig. 5 Typical structures of the acetate anion surrounded by its first solvation shell and the cation (green atom), extracted from $\text{AcO}^- \cdot (\text{H}_2\text{O})_n$ (left)^[64] and $(\text{AcO}^-, \text{K}^+) \cdot (\text{H}_2\text{O})_n$ (middle and right columns) clusters optimised at the RI-B97-D3/dhf-TZVPP level. The type of structure is specified for free acetate ions, SIPs and CIPs (see text for type nomenclature). Water molecules in the first solvation shell around the acetate ion are in ball-and-stick representation, except for cation-anion bridging water molecules which are in stick for SIPs.

Table 1 Simulated frequencies (σ) and corresponding splitting ($\Delta\sigma(\text{CO}_2^-)$) of the carboxylate stretching modes of alkali-metal acetate pairs in aqueous solution (in cm^{-1}). Standard deviations are given in parenthesis for each set.

	Type	$(\text{AcO}^-, \text{Li}^+)$			$(\text{AcO}^-, \text{Na}^+)^{[64]}$			$(\text{AcO}^-, \text{K}^+)$			$(\text{AcO}^-, \text{Rb}^+)$			$(\text{AcO}^-, \text{Cs}^+)$		
		σ^{sym}	σ^{anti}	$\Delta\sigma$	σ^{sym}	σ^{anti}	$\Delta\sigma$	σ^{sym}	σ^{anti}	$\Delta\sigma$	σ^{sym}	σ^{anti}	$\Delta\sigma$	σ^{sym}	σ^{anti}	$\Delta\sigma$
SIP	$^1(3 3)^0$	1422 (4)	1554 (6)	132	1426 (5)	1554 (9)	128	1427 (4)	1557 (8)	130	1427 (6)	1555 (6)	128	1424 (9)	1556 (5)	132
	$^1(3 3)^1$	1427 (5)	1554 (8)	127	1429 (8)	1554 (4)	125	1428 (7)	1553 (9)	125	1428 (6)	1558 (6)	130	1425 (8)	1558 (8)	133
	$^1(3 2)^0$	1419 (9)	1568 (6)	149	1421 (10)	1565 (3)	144	1420 (9)	1571 (9)	151	1421 (12)	1569 (12)	148	1422 (6)	1570 (8)	148
	$^0(3 2)^1$	1425 (5)	1566 (7)	141	1415 (7)	1564 (9)	149	1418 (7)	1566 (6)	148	1417 (9)	1568 (12)	151	1418 (12)	1567 (10)	149
CIP	$(\underline{3} 3)$	1427 (7)	1555 (6)	128	1427 (10)	1553 (6)	126	1424 (4)	1555 (3)	131	1425 (5)	1555 (8)	130	1422 (3)	1558 (7)	136
	$(3 \underline{1}3)$	-	-	-	1425 (11)	1554 (6)	129	1425 (4)	1557 (7)	132	1424 (9)	1557 (4)	133	1420 (6)	1560 (7)	141
	$(\underline{3} 2)$	1419 (7)	1576 (8)	157	1429 (7)	1568 (10)	139	1428 (7)	1566 (9)	138	1425 (8)	1566 (11)	141	1424 (5)	1563 (10)	139
	$(3 \underline{2})$	1425 (7)	1562 (5)	137	1416 (8)	1573 (14)	157	1415 (6)	1578 (11)	163	1413 (9)	1581 (8)	168	1408 (7)	1585 (7)	177
	$(\underline{2} \underline{2})$	1423 (8)	1575 (4)	152	-	-	-	-	-	-	-	-	-	-	-	-

For each of these types, the calculated symmetric ($\sigma(\text{CO}_2^-)^{\text{sym}}$) and antisymmetric ($\sigma(\text{CO}_2^-)^{\text{anti}}$) stretching frequencies are averaged on 5 to 9 different structures and presented in Table 1 (see also Table S4). Several general trends can be observed along the alkali cation series. Firstly, independently of the nature of the cation and the type of ion pairing, symmetric and asymmetric coordination types, labelled 3|3 and 3|2 respectively, have quite different spectral signatures. $\sigma(\text{CO}_2^-)^{\text{sym}}$ and $\sigma(\text{CO}_2^-)^{\text{anti}}$ of 3|2 types tend to be respectively red-shifted and blue-shifted relative to 3|3 types, the latter effect being the most prominent. As a consequence, the splitting between both CO_2^- stretching frequencies ($\Delta\sigma(\text{CO}_2^-) = \sigma(\text{CO}_2^-)^{\text{anti}} - \sigma(\text{CO}_2^-)^{\text{sym}}$) of 3|2 species is thus generally at least 10 cm^{-1} larger than that of 3|3, *i.e.* an asymmetric coordination of the carboxylate group leads to a larger splitting than a symmetric one. Secondly, the spectral signatures of all SIP types, together with that of symmetric $(\underline{3}|3)$ and $(3|\underline{1}3)$ CIP types are largely insensitive to the nature of the cation in view of the variations estimated to only a few cm^{-1} , *i.e.* below the accuracy of these calculations. This can be easily rationalized in the SIP case, where the first solvation shell of carboxylate, composed of water molecules only, is preserved

along the alkali series, thereby explaining the similarities of the vibrational spectra of the CO_2^- stretching modes. In contrast, the spectra of (3|2) and (3|2) CIP types are quite sensitive to the nature of the alkali cation with variations in the 10-20 cm^{-1} range along the cation series. The case of (3|3) and (3|1)3) CIP frequencies which have a cation-dependency similar to SIPs, is more surprising and will be tentatively explained later. These general trends will be especially helpful to infer the coordination of the carboxylate groups in electrolyte solutions.

These results can be compared to the extensive infrared studies that have been published on the relationship between the stretching frequencies of the carboxylate group and its different binding geometries. Among the most significant results, Deacon and Phillips,^[70] by comparing the structures and vibrational frequencies of several crystals of acetate salts where ions are in contact, proposed a widely used diagnosis, which consists of using $\Delta\sigma(\text{CO}_2^-)$ to determine the binding geometries of the CO_2^- group to metal ions, which has proven valid in a few number of simple aqueous systems.^[71] For the simplest case and neglecting all other possible structural and geometric complications, $\Delta\sigma(\text{CO}_2^-)$ is expected to follow the order $\Delta\sigma(\text{CO}_2^-)$ (monodentate) > $\Delta\sigma(\text{CO}_2^-)$ (bidentate).^[70] As shown in Table 1, we verified that this order is still valid for the explicitly solvated structures investigated in our study.

Another more recent theoretical work by Sutton and coworkers^[63] analyzed the C-O bond length/frequency correlations of carboxylate groups using the SMD continuum solvation model.^[72] Similar correlations are found in our study (Fig. 6), but a close examination of our results enables us to extract specific effects of explicit solvation. For all CIPs and SIPs taken together, $\sigma(\text{CO}_2^-)^{\text{sym}}$ decreases and $\sigma(\text{CO}_2^-)^{\text{anti}}$ increases linearly with a significant increase of the C-O bond length difference (δr), echoing the variations already found between the (3|3) and (3|2) types of free acetate ions^[64] (stars in Fig. 6). In (3|3) structures of the free ions, the environment around the CO_2^- group is rather symmetric, leading to similar C-O bond lengths ($\delta r = \sim 0.6$ pm), whereas in the case of (3|2) asymmetric coordination structures, the non-equivalent C-O bonds lead to δr values close to 2.0 pm. While the correlation between $\Delta\sigma(\text{CO}_2^-)$ and δr results intrinsically from the electronic motion of π -electrons capable of strengthening one CO bond while weakening the other one, we note that these parameters reflect the symmetric or asymmetric nature of the environment of the carboxylate probe. Considering ion pairs, the different types appear as two groups nearby the (3|3) and (3|2) structures of the free acetate ion

(stars on Fig. 6): all symmetric coordination types (SIPs ${}^1(3|3)^0$ and ${}^1(3|3)^1$, CIPs $(\underline{3}|3)$ and $(3|\underline{1}3)$) are grouped near the $(3|3)$ type of free acetate (red stars); the asymmetric types (SIPs ${}^1(3|2)^0$ and ${}^0(3|2)^1$, CIPs $(\underline{3}|2)$ and $(3|\underline{2})$) are moderately (SIPs) to largely (CIPs) dispersed around the $(3|2)$ type of the free ion (blue stars). The deviations of the $(3|\underline{2})$ and $(\underline{3}|2)$ types from the free acetate values are thus the most significant, showing that the substitution of a water molecule in a $(3|2)$ type free ion by an alkali-metal cation induces a significant CO_2^- group response, which depends on the nature of the cation. For $(3|\underline{2})$ types, δr increases with the ionic radius of the cation from ~ 1.0 to ~ 3.5 pm, while $\Delta\sigma(\text{CO}_2^-)$ varies from ~ 137 to ~ 177 cm^{-1} . The opposite effect is observed for $(\underline{3}|2)$ types. While substitution of a water molecule by an ion is expected to produce a significant response, it is then remarkable that the analogous substitution of one or two water molecules in a $(3|3)$ type free ion leading to CIPs $(\underline{3}|3)$ or $(3|\underline{1}3)$ structures does not induce any substantial response of the CO_2^- group. This is all the more intriguing as the carboxylate vibrations are known to be intrinsically sensitive to the nature of the alkali cation in a bidentate arrangement as shown on isolated contact ion pairs (~ 20 to 40 cm^{-1} shifts along the alkali series).^[73] It becomes then obvious that, in solution, water molecules are capable to modulate the response of the CO_2^- group up to a point where the formation of a bidentate CIP with an alkali cation may not induce any significant spectral shift of the IR transitions. In conclusion, our study using an explicit solvent shows that the vibrational signature of the carboxylate group does not solely depend on the binding geometry (monodentate or bidentate), and that the complete picture of its first coordination shell must be considered, which justifies *a posteriori* the approach used in this work.

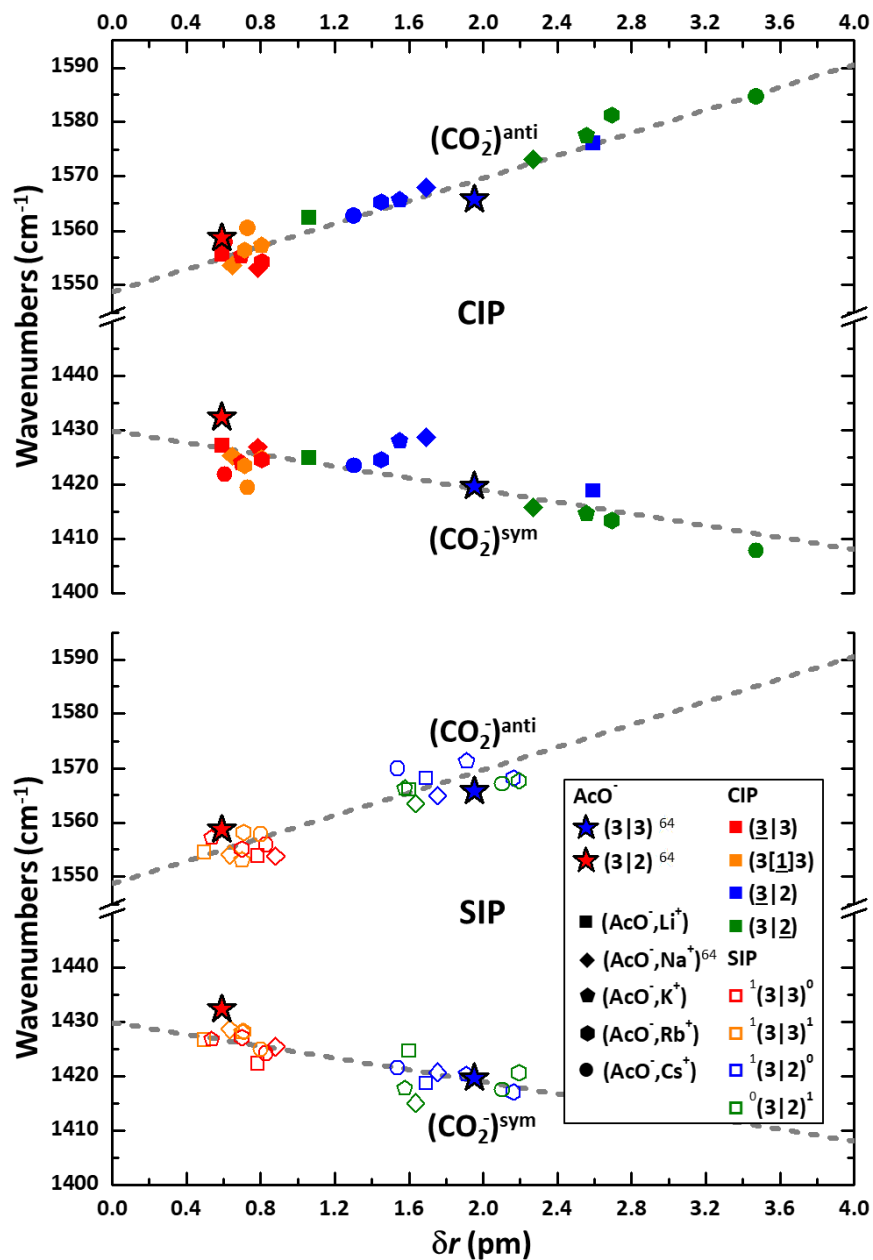


Fig. 6 Correlation between the C-O bond length difference (δr) and the wavenumbers of symmetric $(\text{CO}_2)^{\text{sym}}$ and antisymmetric $(\text{CO}_2)^{\text{anti}}$ stretching modes of the carboxylate group of acetate for CIPs (top) and SIPs (down). These data correspond to the average values calculated from sets of structures for each coordination type (Table 1). Dotted lines are the best linear fits of each mode.

In order to push the analysis further than the carboxylate frequency/structure correlation, we also examined the frequency/electron density correlation by calculating the partial charges of the oxygen atoms of the carboxylate group by means of a NBO analysis at the

RI-B97-D3/dhf-TZVPP level for all systems. Fig. 7 shows the frequency splitting of the CO_2^- stretching modes ($\Delta\sigma(\text{CO}_2^-)$) plotted against the unsigned charge difference between both oxygen atoms of the carboxylate group, $\delta q(\text{O})$, which quantifies the polarization differences of the C-O bonds induced by their local environment. While one could expect that the greater the charge difference $\delta q(\text{O})$, the greater the frequency splitting $\Delta\sigma(\text{CO}_2^-)$, Fig. 7 shows that this statement must be considered with care and only applies within given sets of structures. Indeed, the different coordination types must be sorted in several sets, independently of the nature of the cation. On one side, the symmetric coordination types 3|3 form a rather homogeneous group and display a weak charge difference between both oxygen atoms ($< 0.03 \text{ e}$) (Fig. 7, orange dashed circle), which indicates that the negative charge is equally delocalized between both oxygen atoms of the CO_2^- group in agreement with their relatively similar environments. On the other side, the asymmetric coordination types 3|2 are more spread and have a $\delta q(\text{O})$ generally varying between 0.04 and 0.08 e (Fig. 7, blue dashed circle), except for a few extreme cases. $\delta q(\text{O})$ is significantly larger compared to that of the symmetric coordination types, indicating that the carboxylate C-O bonds are polarized differently. The most negative charge is systematically located on the oxygen atom having the most important coordination number (*i.e.*, 3 here), independently of the position of the cation for CIPs. However, in the latter case, the nature of the cation modulates the asymmetry and has a significant influence on $\delta q(\text{O})$. The asymmetry increases together with the negative charge of the oxygen atom of coordination 3 in ($\underline{3}$ |2) types from Cs^+ ($\delta q(\text{O}) = 0.017 \text{ e}$) to Li^+ (0.104 e) (Fig. 7, blue arrow), and conversely decreases from Cs^+ (0.082 e) to Li^+ (0.021 e) in (3 | $\underline{2}$) coordination types (Fig. 7, green arrow). The nature of the cation is then capable of either amplifying or compensating the intrinsic electronic asymmetry of the carboxylate group in 3|2 structures. It is interesting to note that the $\delta q(\text{O})$ obtained for (AcO^- , Li^+) ($\underline{3}$ |2) and (AcO^- , Cs^+) (3 | $\underline{2}$) types are equivalent to those displayed by the symmetric 3|3 coordination types (orange dashed circle). Considering that $\delta q(\text{O})$ of all these CIPs in solution is comparable to that of a (3 |3) type free acetate ion, these results suggest that, on the one hand, Li^+ polarizes the CO bond like two water molecules in the ($\underline{3}$ |2) type, and that, on the other hand, Cs^+ produces a negligible polarization compared to that of one water molecule in the (3 | $\underline{2}$) type. On this basis, Fig. 7 is consistent with the following classification of the alkali cations according to their ability to polarize the C-O carboxylate bond by taking the water molecule as a reference:

Li^+ (equivalent to two water molecules) > Na^+ (equivalent to one water molecule) \sim $\text{K}^+ \sim \text{Rb}^+ >$ Cs^+ (negligible compared to one water molecule). While this effect has a spectacular impact on the CO_2^- stretch splitting of $(\underline{3}|2)$ or $(3|\underline{2})$ CIPs, it is no longer true for $(\underline{3}|3)$ or $(3|\underline{1}|3)$ structures or SIPs, highlighting again the difficulty to detect these types using IR spectroscopy.

More generally, this whole study reveals how paired and free acetate ions can coincidentally yield surprisingly close vibrational signatures, echoing an observation made on microsolvated carboxylate groups, free or paired with a doubly charge metal cation.^[51] These results illustrate the challenge to monitor ion pairing by IR spectroscopy, as already seen for sodium acetate.^[64] Nevertheless, such a theoretical study taking into account explicit solvation is a precious help to finely compare the CO_2^- stretch vibrations of the ion pairs with those of free acetate ions in order to predict the spectral shifts induced by ion pairing.

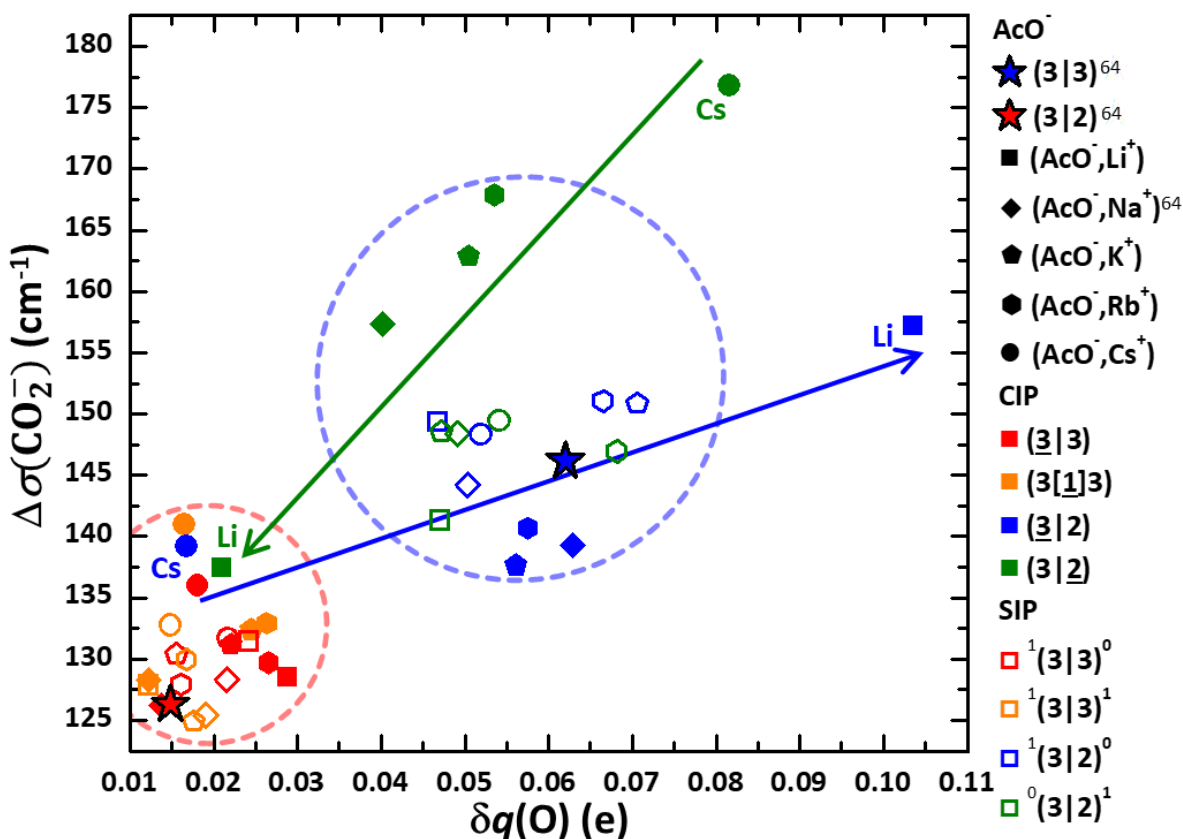


Fig. 7 Frequency splitting of the carboxylate stretching modes $\Delta\sigma(\text{CO}_2^-)$ as a function of the unsigned charge difference between both oxygen atoms of carboxylate $\delta q(\text{O})$, determined by NBO analysis at the RI-B97-D3/dhf-TZVPP level, for all coordination types of each cluster. Dashed circles represent two sets with different coordination types: the symmetric coordination types $3|3$ in orange and the asymmetric coordination types $3|2$ in blue. The blue

arrow highlights the increase of asymmetry from Cs⁺ to Li⁺ in (3|2) coordination types, and the green arrow its decrease in the case of (3|2) types.

For this purpose, Fig. 8 presents the shifts of $\sigma(\text{CO}_2^-)^{\text{sym}}$ and $\sigma(\text{CO}_2^-)^{\text{anti}}$ observed between ion pairs and free ions (see also Table S5). This figure aims at interpreting the shifts observed in an experiment where the equilibrium between the free ions and the ion pairs is shifted towards ion pair formation, *e.g.* when the ionic concentration increases. Several trends can be identified, providing that symmetric 3|3 and asymmetric 3|2 coordination type populations are first considered to be independent. Regarding the formation of SIP and CIP from free acetate ions (3|3), symmetric coordination types (¹(3|3)⁰, ¹(3|3)¹, (3|3) and (3|1|3)) lead almost exclusively to a red-shift of both CO₂⁻ stretching frequencies, the most significant values being comprised between 4 and 12 cm⁻¹ for the symmetric mode, whatever the cation considered. On the other side, for each cation, the signatures of the different types differ by a few wavenumbers, making all these ion pairs potentially indistinguishable from each other by IR spectroscopy as already mentioned.

For the asymmetric coordination types, ¹(3|2)⁰ and ⁰(3|2)¹ structures have the same frequencies as free acetate in general, although relatively small shifts of $\sigma(\text{CO}_2^-)^{\text{anti}}$ or $\sigma(\text{CO}_2^-)^{\text{sym}}$ may occasionally be observed depending on the nature of the cation. IR spectroscopy may thus not be very sensitive to the formation of these SIPs. In contrast, (3|2) and mostly (3|2) CIPs show large blue- or red-shifts, which strongly depend on the nature of the cation.

From these theoretical results, SIP formation from free ions is expected to induce a measurable red-shift of the two CO₂⁻ stretching bands, mainly resulting from the pairing of (3|3) structures as already observed in the case of Na⁺,^[64] whereas CIP formation of (3|2) and (3|2) species from (3|2) free ions should contribute to red- or blue-shift CO₂⁻ stretching frequencies depending on the nature of the cation. However, this ideal picture where symmetric 3|3 and asymmetric 3|2 coordination types are considered separately may be blurred by acetate population transfer between these two categories when the concentration is increased in an experiment. In this respect, Fig. 7 shows that $\Delta\sigma(\text{CO}_2^-)$ is a good indicator to monitor these population transfers as 3|2 coordination types for each cation have quasi-systematically larger splittings than 3|3 types. Both the shift of the CO₂⁻ stretching bands and the frequency splitting $\Delta\sigma(\text{CO}_2^-)$ will then be

used to propose an ion pair assignment from IR spectroscopy measurements of solutions of increasing concentration.

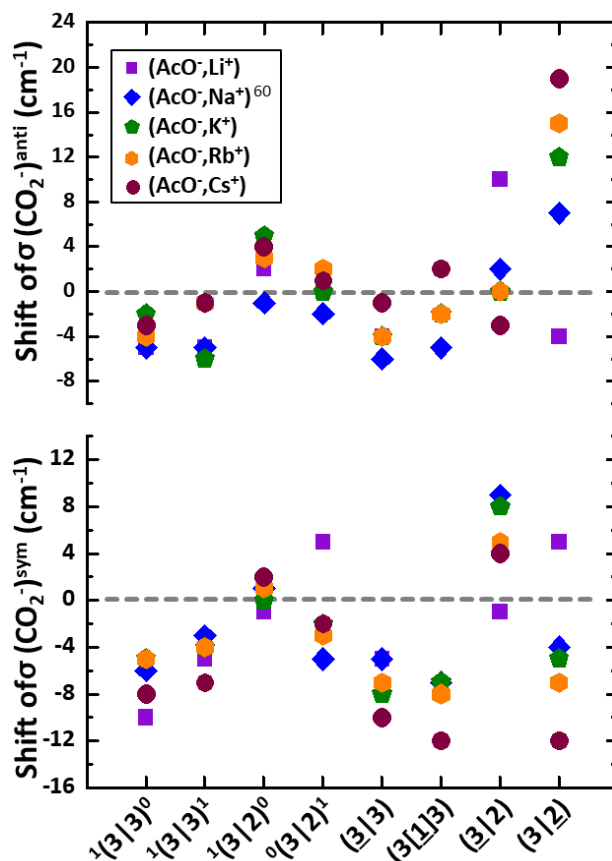


Fig. 8 Shifts of $\sigma(\text{CO}_2^-)^{\text{sym}}$ and $\sigma(\text{CO}_2^-)^{\text{anti}}$ of each coordination type from theoretical values of free acetate ions obtained at the same level of theory:^[64] $\sigma(\text{CO}_2^-)^{\text{sym}} = 1432 \text{ cm}^{-1}$ and $\sigma(\text{CO}_2^-)^{\text{anti}} = 1559 \text{ cm}^{-1}$ values from (3|3) free ions are taken as references for 3|3 symmetric coordination types; $\sigma(\text{CO}_2^-)^{\text{sym}} = 1420 \text{ cm}^{-1}$ and $\sigma(\text{CO}_2^-)^{\text{anti}} = 1566 \text{ cm}^{-1}$ from (3|2) free ions are taken for 3|2 types.

Comparison between experimental and theoretical IR data

ATR-FTIR results led us to distinguish low ($< \sim 2 \text{ M}$) and high ($> \sim 2 \text{ M}$) concentration regions. Several arguments already plead in favour of the presence of SIP in the low concentration region (section ATR-FTIR Studies). Our theoretical study showed moreover that an acetate population transfer from free ions to SIPs should likely lead to a red-shift of both transitions (Fig. 8), which is indeed observed when concentration is increased (Fig. 1). It is therefore legitimate to analyse

the low concentration region by considering that acetate ions are either free or paired within SIPs species only.

From the first experimental point around 0.2 M, slight shifts from free acetate frequencies are observed, indicating the presence of SIPs in measurable amount. The linearity up to ~ 2 M (Fig. 1) is consistent with a continuously increasing concentration of SIP species. In particular, there is no evidence of concentration thresholds that could be associated either with the onset of their formation, or with significant changes within SIP distributions. Spectral shifts will thus be interpreted as resulting uniquely from a SIP concentration increase, the changes of the SIP distribution being neglected along the whole concentration range. According to the theoretical study presented above, the experimental shifts can be assigned to the formation of specific types of SIPs, providing that acetate population transfers between symmetric 3|3 and asymmetric 3|2 types during ion pairing can be neglected. This assumption is indeed largely supported by the modest change of splitting experimentally observed for all cations up to 2 M (~ 1 cm⁻¹, Fig. 9a) compared to that resulting from a complete population transfer (~ 15 cm⁻¹ between the blue star and the orange and red open symbols of Fig. 7).

Based on the above theoretical analysis (Fig. 8), the red-shift of the $(\text{CO}_2^-)^{\text{sym}}$ and $(\text{CO}_2^-)^{\text{anti}}$ transitions at low concentration (Fig. 1) is fully consistent with the formation of $^1(3|3)^0$ or $^1(3|3)^1$ SIPs from (3|3) free ions. In contrast, the formation of $^1(3|2)^0$ and $^0(3|2)^1$ SIPs from (3|2) free ions is predicted to either not producing any significant shift, or rarely induce blue shifts contrary to the observation. It is then likely that $^1(3|3)^0$ or $^1(3|3)^1$ SIPs dominate the $^1(3|2)^0$ and $^0(3|2)^1$ species. Interestingly, cation-specific shifts of the $(\text{CO}_2^-)^{\text{sym}}$ transition are observed when SIPs are formed, but they remain too small (less than ~ 1 cm⁻¹) to be captured by our theoretical study. It is thus difficult to assign this behaviour either to a cation-specific spectroscopic property of the SIPs, or to a cation-specific SIP formation rate as the concentration increases. In turn, the experimental splitting (Fig. 9a) is found to either slightly decrease for the lighter cations (Li^+ , Na^+ and K^+) or slightly increase for the heavier (Rb^+ and Cs^+) in the SIP concentration region, the increase of the slope of the linear fit (dashed lines in the left part of Fig. 9a) remarkably following the alkali cation series from Li^+ to Cs^+ . While the formation of most SIPs from (3|2) or (3|3) free ions increases the splitting (Fig. 9b) as observed for Rb^+ and Cs^+ , the decrease of splitting observed for Li^+ , Na^+ and K^+ is only supported by a very limited number of SIPs

according to Fig. 9b. One cannot exclude that a modest population transfer from symmetric 3|3 to asymmetric 3|2 coordination types could also be responsible for this decrease of splitting.

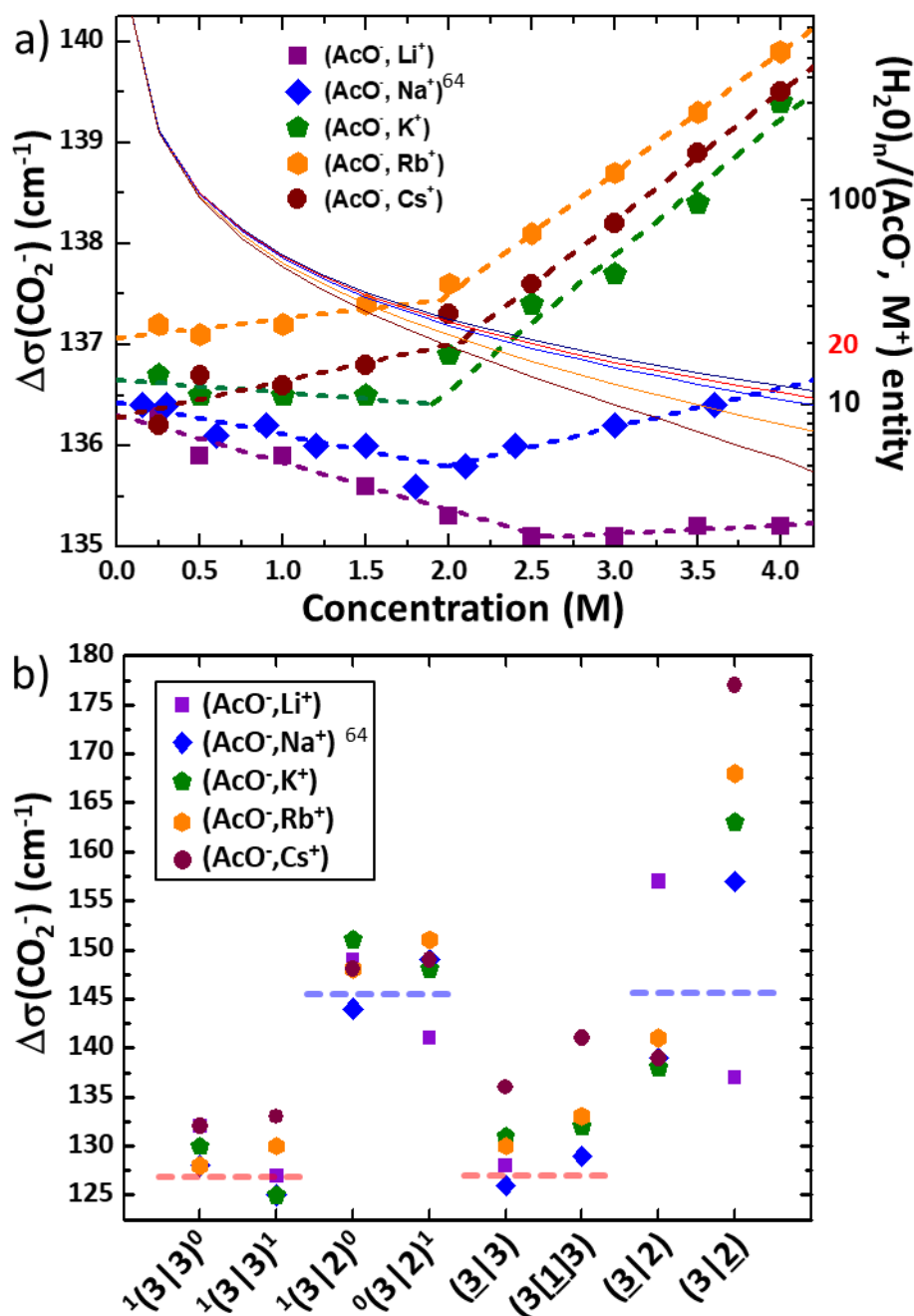


Fig. 9 (a) Experimental splitting of the carboxylate stretching modes $\Delta\sigma(\text{CO}_2^-)$ (dots), and number of water molecules available per alkali acetate entity (solid lines) as a function of ion concentration, where dashed lines are lines of best fit passing through low and high concentration subsets. (b) Calculated frequency splitting of the carboxylate stretching modes for all spectroscopic types, where red and blue horizontal dashed lines indicate the values calculated for the (3|3) and (3|2) types of free acetate ions, respectively.

As concentration increases from ~2 to 4 M, where CIPs and higher-order contact clusters must be formed according to the number of water molecules available per (AcO^- , M^+) entity (Fig. 9a), the transitions still redshift but to a lesser or greater degree for $(\text{CO}_2^-)^{\text{anti}}$ and $(\text{CO}_2^-)^{\text{sym}}$ respectively (Fig. 1), indicating the appearance of new structures that are absent at lower concentration. This change of slope, which is simultaneous on both transitions for $\text{M} = \text{Li}, \text{K}, \text{Rb}$ and Cs (not visible for Na $(\text{CO}_2^-)^{\text{sym}}$), is even more clearly seen on the splitting (Fig. 9a) and may be interpreted as a consequence of the presence of CIPs and/or higher-order contact clusters. This concentration threshold for CIP appearance occurs in the 1.9 - 2.1 M range for all cations, except for Li^+ for which it is observed at 2.6 ± 0.1 M. The decreasing rate of red-shift of the $(\text{CO}_2^-)^{\text{anti}}$ transition above this threshold can be correlated with the formation of CIPs from SIPs. Indeed, Fig. 8 shows that CIPs induce either moderate red-shifts similar to those observed during SIP formation, *e.g.* in the case of $(\underline{3}|\underline{3})$ or $(3|\underline{1}|\underline{3})$ CIPs, or sometimes significant blue-shifts, such as $(3|\underline{2})$ CIPs for Na^+ , K^+ , Rb^+ and Cs^+ , or $(\underline{3}|\underline{2})$ CIPs for Li^+ . The simultaneous appearance of these CIPs could thus result in the smaller redshift rate observed. For the $(\text{CO}_2^-)^{\text{sym}}$ transition however, the unchanged or slightly increased red-shift rate suggests a better compatibility with $(\underline{3}|\underline{3})$ or $(3|\underline{1}|\underline{3})$ than the other CIPs according to Fig. 8. For this high concentration range ($> \sim 2$ M), the experimental splitting increases (Fig. 9), slightly for $(\text{AcO}^-$, $\text{Li}^+)$ and $(\text{AcO}^-$, $\text{Na}^+)$, and more significantly for the other systems. Multiple causes may explain this behaviour, such as the contribution of specific CIPs, like *e.g.* $(3|\underline{2})$, or population transfers from $3|\underline{3}$ to $3|\underline{2}$ coordination types. In addition, the number of water molecules above ~ 3 M is no longer sufficient (< 14 per $(\text{AcO}^-$, $\text{M}^+)$ entity, see Fig. 9a) to complete the first solvation shell around the most compact ion pairs, leading to the formation of larger clusters whose IR signature has not been investigated.

Interestingly, these results infrim some conclusions of previous works. First, the FTIR spectra obtained for $(\text{AcO}^-$, $\text{Na}^+)$ solutions differ significantly from those achieved by Rudolph *et al.*^[37], who reported no pronounced change of the carboxylate stretch transition up to 5 M in contradiction with their expectation if CIPs were formed. As we pointed out in a previous article,^[64] the differences between the operating conditions, and especially the use of the more appropriate ATR-FTIR technique may explain the difference between both datasets. In addition, spectra of a 0.93 M lithium acetate and 13.56 M lithium chloride solution displayed a transition at $\sim 1440\text{-}1444$ cm^{-1} , which was assigned to $\sigma(\text{CO}_2^-)^{\text{sym}}$ of $(\text{AcO}^-$, $\text{Li}^+)$ CIPs assuming a bidentate

type of binding.^[37] Our theoretical and experimental studies both contradict this assignment since, on the one hand, these bidentate ion pairs are not predicted to be stable enough in solution at room pressure and temperature operating conditions and, on the other hand, such a solution contains large ionic clusters which must be responsible for such a $\sigma(\text{CO}_2^-)^{\text{sym}}$ transition that is incompatible with both our measurements at high concentrations and our frequency calculations on CIPs. Regarding the evolution of the concentration threshold of CIP appearance with the alkali cation ($\text{Cs}^+ \sim \text{Rb}^+ \sim \text{K}^+ \sim \text{Na}^+ < \text{Li}^+$), it is in apparent contradiction with the Collins' "law of matching water affinities".^[13] Following this widely-used principle, systems with moderate solubility are deemed to have a strong tendency to form CIPs, whereas systems with high solubility tend to form mostly SIPs (solubility in H_2O at 25°C : $(\text{AcO}^-, \text{Li}^+) = 6.8 \text{ mol/L}$; $(\text{AcO}^-, \text{Na}^+) = 6.1 \text{ mol/L}$; $(\text{AcO}^-, \text{K}^+) = 27.3 \text{ mol/L}$).^[74] Our measured thresholds (Fig. 1 and 9) display a different picture, showing that solubility thresholds are not good indicators for estimating CIP appearance thresholds. Finally, it should be noted that Hess and van der Vegt^[48] found that the ion pairing interaction order between carboxylate and alkali atoms follows the Hofmeister series $\text{K}^+ < \text{Na}^+ < \text{Li}^+$ due to their relative propensity to form SIPs vs. CIPs, which is in line with the SIP concentration ranges observed in our study, $\text{K}^+ \sim \text{Na}^+ < \text{Li}^+$.

Conclusion

In this work, we have demonstrated that the structure of the carboxylate-alkali cations ($\text{M} = \text{Li}, \text{Na}, \text{K}, \text{Rb}, \text{Cs}$) pairs in solution is dependent on the nature of the cation and their interactions with the first shell of solvent molecules. Theoretical simulations in explicit solvent at a high level of theory coupled to ATR-FTIR experiments revealed several spectral signatures consistent with the formation of ion pairs from the dilute to the concentrated regime where the anion-cation interactions take a critical part in the supramolecular organization of the solution.

On the experimental side, the measurement of spectral quantities ($\sigma(\text{CO}_2^-)^{\text{sym}}$, $\sigma(\text{CO}_2^-)^{\text{anti}}$ and $\Delta\sigma(\text{CO}_2^-)$) for different systems ($(\text{AcO}^-, \text{M}^+)$; $\text{M} = \text{Li}, \text{Na}, \text{K}, \text{Rb}$ and Cs) as a function of the concentration provided several benchmarks. The accuracy of the measurements and the consistency of all datasets allowed us to extrapolate the signature of free acetate ions ($\sigma^0(\text{CO}_2^-)^{\text{sym}} = 1415.1 \pm 0.3$ and $\sigma^0(\text{CO}_2^-)^{\text{anti}} = 1551.5 \pm 0.3 \text{ cm}^{-1}$) at infinite dilution (0 M).

Quantitatively, spectral shifts ($\sim 2\text{-}6\text{ cm}^{-1}$) were monitored as the ion concentration increases, and change in shift slopes were observed and assigned to CIP appearance concentration thresholds ($2.6 \pm 0.1\text{ M}$ for AcO^- , Li^+ , and in the $1.9\text{ - }2.1\text{ M}$ range for the other systems). In particular, these concentration thresholds do not correlate with the ion-pairing preferences expected from the Collins classification.^[13] These experimental results also highlight the advantage of ATR-FTIR spectroscopy, which can supply information about the signature of the carboxylate probe with enough sensitivity to monitor SIP formation from the free ions. ATR-FTIR is certainly among the fastest and easiest methods to obtain such an information.

A more comprehensive insight has been obtained by comparing these measurements to the theoretical study. Simulations in explicit solvent model at high level of theory provided invaluable benchmark data for the carboxylate-alkali metal ion pairs in solution, thus constituting relevant guidelines for the interpretation of IR spectra. Both the shifts of the CO_2^- symmetric and antisymmetric stretching bands and the frequency splitting $\Delta\sigma(\text{CO}_2^-)$ were used to narrow down the identification of the environment of the CO_2^- group, and thus the type of ion pairs formed. Spectral shifts from the free ion transitions are found to be weakly dependent on the cation for SIPs [-10 ; $+5\text{ cm}^{-1}$], these differences being more pronounced and dispersed [-12 ; $+19\text{ cm}^{-1}$] in the case of CIPs. The quality of the simulations in explicit solvent is highlighted by the good correlations found between geometric parameters and stretching frequencies of the CO_2^- group, as well as between the charge difference $\delta q(\text{O})$ and the frequency splitting $\Delta\sigma(\text{CO}_2^-)$, thus allowing a rationalization of the structural and electronic response of the CO_2^- group to ion pairing. In particular, these investigations emphasized the significant role of the water molecules of the first two solvation shells around the carboxylate when a precise prediction of its vibrational signature is targeted. Together, these results point out the requirements and benefits of the combination of advanced theoretical calculations and spectroscopic measurements of molecular probes for an in-depth investigation of the supramolecular structures of electrolyte solutions.

Experimental section

Lithium acetate dihydrate, sodium acetate and potassium acetate were obtained from Prolabo (Normapur® grade). Cesium acetate was obtained from Alfa Aesar (99.9% metals basis). Rubidium acetate was obtained from ABCR (99.8% metals basis) and was heated at 140 °C for 3 h in an open crystallizing dish to remove residual acetic acid. Concentrated stock solutions (range 4-6 M) were prepared by dissolving the appropriate amount of each salt in pure water (Rephile PURIST®). Stock solutions were used to prepare sets of sample solutions with concentrations of 0.25, 0.5, 1.0, 1.5, 2.0, 2.5, 3.0, 3.5 and 4.0 M.

A Perkin-Elmer Spectrum Two infrared spectrometer was used for ATR-FTIR (Attenuated Total Reflectance–Fourier Transform Infrared) analysis. The sampling station was fitted with an overhead universal ATR accessory featuring a chemical inert, single reflection synthetic diamond crystal. A 5 μL aliquot of each sample solution was deposited on the ATR diamond for analysis. Due to the strong absorbance of water in the mid-infrared spectral region, the IR difference spectra were considered, taking pure water as a reference. ATR-FTIR spectra of the samples were recorded in a wavenumber range from 1300 cm^{-1} to 1650 cm^{-1} , and corrected against the background spectrum of water, to present the spectra in absorbance units. All spectral measurements were carried out at room temperature and scans were acquired with an analysis interval of 0.2 cm^{-1} and a spectral resolution of 4 cm^{-1} .

Computational methods

The approach combining molecular simulations and quantum chemical calculations is analogous to that developed and validated in a previous study on the free acetate ion and its pairs with a sodium ion in solution.^[64] This approach aims at obtaining the individual vibrational spectra of each type of pairs with enough accuracy to compare them with experimental spectra and provide a structural assignment of ion pairs in solution.

The approach is based on a cluster model containing both ions and several shells of explicit solvent molecules, and consists of three main steps: (i) exploration of the potential energy surface in order to identify low-energy local minima using the polarizable force field AMOEBA combined to a non-local optimization method,^[75] (ii) geometry optimization at the RI-B97-

D3/dhf-TZVPP level of selected structures; and (iii) harmonic frequency calculations using the same quantum chemistry method, followed by a mode-dependent scaling procedure previously determined from gas phase experimental measurements on isolated CIPs, in order to compensate for anharmonicity effects and other systematic errors of the theoretical method.^[64]

Briefly, the potential energy surface of ion pairs solvated in a water cluster with N water molecules ($(\text{AcO}^-, \text{M}^+) \cdot (\text{H}_2\text{O})_N$; $\text{M} = \text{Li, K, Rb and Cs}$; $N \in [260; 540]$) was explored using the polarizable force field AMOEBA combined to the biased Monte-Carlo minimisation algorithm developed by Scheraga^[76] implemented in TINKER.^[77] These clusters were made of two parts: (i) a conformationally explored core containing the acetate anion and the desired cation, surrounded by at least three shells of explicit water molecules, and (ii) an external domain made of several hundreds of water molecules (typically two shells) frozen in a AMOEBA minimum geometry (ESI, Fig. S1). AMOEBA parameters for alkali-metal cations were not available in the literature, except for sodium,^[75] they were therefore built for this purpose (Section S1). From the minima found by the exploration, sampling was then carried out to select representative structures.

In the second step, the core of these selected structures, *i.e.* the ions and typically three hydration shells with n water molecules, was extracted to define starting structures $(\text{AcO}^-, \text{M}^+) \cdot (\text{H}_2\text{O})_n$; $n \in [100; 150]$) for geometry optimisations. The inner part, *i.e.* the ions and their first two solvation shells, surrounded by a frozen solvation shell and the solvent continuum model COSMO^[78] (Fig. S1) was optimized at the RI-DFT-D3/dhf-TZVPP level, using the TURBOMOLE package.^[79] The need to consider the first two solvation shells for an accurate vibrational frequency predictions is notably supported by recent results.^[51] In order to ensure adequate convergence and reliability of the computed frequencies, tight optimization convergence criteria and fine integration grids were used (Section S3).

Finally, harmonic frequencies were calculated for a limited number of degrees of freedom, with the same quantum chemistry method used previously for the optimization step, without the continuum solvent model. Theoretical frequencies were thus scaled using mode-dependent scaling functions.^[64] It was previously shown that this approach lead to an accurate frequency prediction for the carboxylate symmetric and antisymmetric stretching modes, labelled $(\text{CO}_2^-)^{\text{sym}}$ and $(\text{CO}_2^-)^{\text{anti}}$ respectively, *i.e.* with an error of typically $\pm 15 \text{ cm}^{-1}$ for $\sigma(\text{CO}_2^-)^{\text{sym}}$ and $\pm 5 \text{ cm}^{-1}$ for $\sigma(\text{CO}_2^-)^{\text{anti}}$.

Further details on the theoretical approach can be found in ref.^[64] and in Sections S1-S3.

Supporting information

Electronic supporting information (ESI) available: S1 AMOEBA parameters; S2 Theoretical approach; S3 DFT-D calculations; S4 ATR-FTIR spectra. S5 Ion pairs structures obtained at the the AMOEBA polarizable force field level and the RI-B97-D3/dhf-TZVPP level; S6 Mode-dependent scaled harmonic frequency calculations in solution at the RI-B97-D3/dhf-TZVPP level;

Acknowledgments

Authors gratefully thank ANR (grant ANR-16-CE29-0017) and GENCI-TGCC and CCRT (projects A0050807524 and p615) for their support.

References

- [1] N. F. A. van der Vegt, K. Haldrup, S. Roke, J. R. Zheng, M. Lund, H. J. Bakker *Chem. Rev.* **2016**, *116*, 7626-7641.
- [2] M. O. de la Cruz, L. Belloni, M. Delsanti, J. P. Dalbiez, O. Spalla, M. Drifford *J. Chem. Phys.* **1995**, *103*, 5781-5791.
- [3] M. R. Sambrook, P. D. Beer, J. A. Wisner, R. L. Paul, A. R. Cowley, F. Szemes, M. G. B. Drew *J. Am. Chem. Soc.* **2005**, *127*, 2292-2302.
- [4] M.-J. Han, Y.-M. Chen, K.-Z. Wang *New J. Chem.* **2008**, *32*, 970-980.
- [5] R. Billing, D. Rehorek, H. Hennig *Top. Curr. Chem.* **1990**, *158*, 151-199.
- [6] R. J. Forster, L. R. Faulkner *J. Am. Chem. Soc.* **1994**, *116*, 5444-5452.
- [7] V. A. Grigoriev, D. Cheng, C. L. Hill, I. A. Weinstock *J. Am. Chem. Soc.* **2001**, *123*, 5292-5307.
- [8] B. H. Honig, W. L. Hubbell *Proc. Natl. Acad. Sci. USA* **1984**, *81*, 5412-5416.
- [9] H. Bian, H. Chen, Q. Zhang, J. Li, X. Wen, W. Zhuang, J. Zheng *J. Phys. Chem. B* **2013**, *117*, 7972-7984.

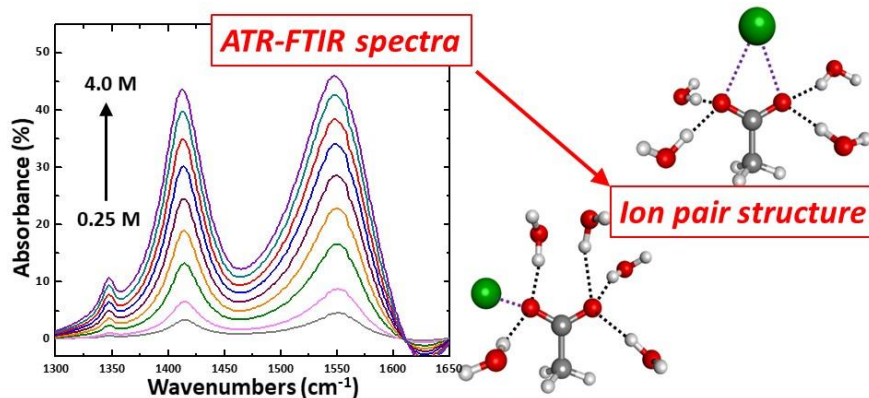
- [10] C. Allolio, N. Salas-Illanes, Y. S. Desmukh, M. R. Hansen, D. Sebastiani *J. Phys. Chem. B* **2013**, *117*, 9939-9946.
- [11] M. H. Shamsi, H.-B. Kraatz *J. Inorg. Organomet. Polym. Mater.* **2013**, *23*, 4-23.
- [12] K. M. Anderson, A. Esadze, M. Manoharan, R. Brüscheiler, D. G. Gorenstein, J. Iwahara *J. Am. Chem. Soc.* **2013**, *135*, 3613-3619.
- [13] K. D. Collins *Biophys. J.* **1997**, *72*, 65-76.
- [14] R. Buchner, T. Chen, G. Hefter *J. Phys. Chem. B* **2004**, *108*, 2365-2375.
- [15] Y. Marcus, G. Hefter *Chem. Rev.* **2006**, *106*, 4585-4621.
- [16] R. M. Fuoss *Proc. Natl. Acad. Sci. USA* **1980**, *77*, 34-38.
- [17] C. B. Monk, C. V. King *J. Electrochem. Soc.* **1961**, *108*, 247C.
- [18] G. H. Nancollas, Interactions in electrolyte solutions: Metal complex and ion-pair formation in solution, Elsevier Pub. Co., **1966**.
- [19] C. B. Chan, N. H. Tioh, G. T. Hefter *Polyhedron* **1984**, *3*, 845-851.
- [20] A. V. McCormick, A. T. Bell, C. J. Radke *J. Phys. Chem.* **1989**, *93*, 1733-1737.
- [21] E. N. W. Howe, M. Bhadbhade, P. Thordarson *J. Am. Chem. Soc.* **2014**, *136*, 7505-7516.
- [22] F. Alkan, T. Small, S. Bai, A. Dominowski, C. Dybowski *J. Struct. Chem.* **2016**, *57*, 369-375.
- [23] C. D'Agostino, M. D. Mantle, C. L. Mullan, C. Hardacre, L. F. Gladden *ChemPhysChem* **2018**, *19*, 1081-1088.
- [24] S. H. Mohamed, Y. M. Issa, S. A. Elfeky, A. A. Ahmed, N. S. Abdelkader *J. Mol. Struct.* **2020**, 128074.
- [25] A. Bonsen, W. Knoche, W. Berger, K. Giese, S. Petrucci *Ber. Bunsenges. Phys. Chem.* **1978**, *82*, 678-683.
- [26] U. Kaatze, T. O. Hushcha, F. Eggert *J. Solution Chem.* **2000**, *29*, 299.
- [27] R. Buchner, F. Samani, P. M. May, P. Sturm, G. Hefter *ChemPhysChem* **2003**, *4*, 373-378.
- [28] W. Wachter, Š. Fernandez, R. Buchner, G. Hefter *J. Phys. Chem. B* **2007**, *111*, 9010-9017.
- [29] R. Buchner, G. Hefter *Phys. Chem. Chem. Phys.* **2009**, *11*, 8984-8999.

- [30] E. F. Aziz, A. Zimina, M. Freiwald, S. Eisebitt, W. Eberhardt *J. Chem. Phys.* **2006**, *124*, 114502.
- [31] J. S. Uejio, C. P. Schwartz, A. M. Duffin, W. S. Drisdell, R. C. Cohen, R. J. Saykally *Proc. Natl. Acad. Sci. U. S. A.* **2008**, *105*, 6809-6812.
- [32] E. F. Aziz, N. Ottosson, S. Eisebitt, W. Eberhardt, B. Jagoda-Cwiklik, R. Vacha, P. Jungwirth, B. Winter *J. Phys. Chem. B* **2008**, *112*, 12567-12570.
- [33] C. S. Oliveira, K. P. Branco, M. S. Baptista, G. L. Indig *Spectroc. Acta A* **2002**, *58*, 2971-2982.
- [34] G. Heftner *Pure Appl. Chem.* **2006**, *78*, 1571-1586.
- [35] F. Sebe, K. Nishikawa, Y. Koga *Phys. Chem. Chem. Phys.* **2012**, *14*, 4433.
- [36] Z. Sun, W. Zhang, M. Ji, R. Hartsock, K. J. Gaffney *J. Phys. Chem. B* **2013**, *117*, 15306-15312.
- [37] W. W. Rudolph, D. Fischer, G. Irmer *Dalton trans.* **2014**, *43*, 3174-3185.
- [38] J. Tandy, C. Feng, A. Boatwright, G. Sarma, A. M. Sadoon, A. Shirley, N. D. Rodrigues, E. M. Cunningham, S. F. Yang, A. M. Ellis *J. Chem. Phys.* **2016**, *144*, 121103.
- [39] A. Sthoer, J. Hladílková, M. Lund, E. Tyrode *Phys. Chem. Chem. Phys.* **2019**, *21*, 11329-11344.
- [40] A. Sthoer, E. Tyrode *J. Phys. Chem. C* **2019**, *123*, 23037-23048.
- [41] E. Weißenborn, B. Braunschweig *Molecules* **2019**, *24*, 2911.
- [42] M. Berkowitz, O. A. Karim, J. A. McCammon, P. J. Rossky *Chem. Phys. Lett.* **1984**, *105*, 577-580.
- [43] B. M. Pettitt, P. J. Rossky *J. Chem. Phys.* **1986**, *84*, 5836-5844.
- [44] I. Harsányi, L. Pusztai *J. Chem. Phys.* **2005**, *122*, 124512.
- [45] C. J. Fennell, A. Bizjak, V. Vlachy, K. A. Dill *J. Phys. Chem. B* **2009**, *113*, 6782-6791.
- [46] J. Timko, D. Bucher, S. Kuyucak *J. Chem. Phys.* **2010**, *132*, 114510.
- [47] M. K. Ghosh, S. Re, M. Feig, Y. Sugita, C. H. Choi *J. Phys. Chem. B* **2013**, *117*, 289-295.
- [48] B. Hess, N. F. A. van der Vegt *Proc. Natl. Acad. Sci. U. S. A.* **2009**, *106*, 13296-13300.

- [49] P. Jungwirth *J. Phys. Chem. B* **2014**, *118*, 10333-10334.
- [50] C. J. Johnson, L. C. Dzugan, A. B. Wolk, C. M. Leavitt, J. A. Fournier, A. B. McCoy, M. A. Johnson *J. Phys. Chem. A* **2014**, *118*, 7590-7597.
- [51] J. K. Denton, P. J. Kelleher, M. A. Johnson, M. D. Baer, S. M. Kathmann, C. J. Mundy, B. A. W. Rudd, H. C. Allen, T. H. Choi, K. D. Jordan *Proc. Natl. Acad. Sci. U. S. A.* **2019**, *116*, 14874-14880.
- [52] J. W. DePalma, P. J. Kelleher, L. C. Tavares, M. A. Johnson *J. Phys. Chem. Lett.* **2017**, *8*, 484-488.
- [53] J.-H. Choi, H. R. Choi, J. Jeon, M. Cho *J. Chem. Phys.* **2017**, *147*, 154107.
- [54] Y. Marcus *Chem. Rev.* **2009**, *109*, 1346-1370.
- [55] A. W. Omta, M. F. Kropman, S. Woutersen, H. J. Bakker *Science* **2003**, *301*, 347-349.
- [56] P. Schienbein, G. Schwaab, H. Forbert, M. Havenith, D. Marx *J. Phys. Chem. Lett.* **2017**, *8*, 2373-2380.
- [57] A. Shalit, S. Ahmed, J. Savolainen, P. Hamm *Nat. Chem.* **2017**, *9*, 273-278.
- [58] J. Kahlen, L. Salimi, M. Sulpizi, C. Peter, D. Donadio *J. Phys. Chem. B* **2014**, *118*, 3960-3972.
- [59] K. D. Collins *Biophys. Chem.* **2006**, *119*, 271-281.
- [60] K. D. Collins *Biophys. Chem.* **2012**, *167*, 43-59.
- [61] F. R. Beierlein, T. Clark, B. Braunschweig, K. Engelhardt, L. Glas, W. Peukert *J. Phys. Chem. B* **2015**, *119*, 5505-5517.
- [62] M. Nara, H. Torii, M. Tasumi *J. Phys. Chem.* **1996**, *100*, 19812-19817.
- [63] C. C. R. Sutton, G. da Silva, G. V. Franks *Chem. Eur. J.* **2015**, *21*, 6801-6805.
- [64] S. Habka, T. Very, J. Donon, V. Vaquero-Vara, B. Tardivel, F. Charnay-Pouget, M. Mons, D. J. Aitken, V. Brenner, E. Gloaguen *Phys. Chem. Chem. Phys.* **2019**, *21*, 12798-12805.
- [65] W. W. Rudolph, G. Irmer *RSC Adv.* **2015**, *5*, 21897-21908.
- [66] M. V. Fedotova, S. E. Kruchinin *J. Mol. Liq.* **2011**, *164*, 201-206.
- [67] S. Varma, S. B. Rempe *Biophys. Chem.* **2006**, *124*, 192-199.
- [68] C. J. Carrell, H. L. Carrell, J. Erlebacher, J. P. Glusker *J. Am. Chem. Soc.* **1988**, *110*, 8651-8656.

- [69] R. D. Shannon *Acta Crystallogr., Sect. A: Found. Crystallogr.* **1976**, *32*, 751-767.
- [70] G. Deacon, R. J. Phillips *Coord. Chem. Rev.* **1980**, *33*, 227-250.
- [71] J. E. Tackett *Appl. Spectrosc.* **1989**, *43*, 483-489.
- [72] A. V. Marenich, C. J. Cramer, D. G. Truhlar *J. Phys. Chem. B* **2009**, *113*, 6378-6396.
- [73] J. Donon, S. Habka, V. Vaquero-Vara, V. Brenner, M. Mons, E. Gloaguen *J. Phys. Chem. Lett.* **2019**, *10*, 7458-7462.
- [74] D. R. Lide, CRC Handbook of Chemistry and Physics, 82nd Edition, CRC Press, **2001**.
- [75] M. L. Laury, L. P. Wang, V. S. Pande, T. Head-Gordon, J. W. Ponder *J. Phys. Chem. B* **2015**, *119*, 9423-9437.
- [76] L. Piela, J. Kostrowicki, H. A. Scheraga *J. Phys. Chem.* **1989**, *93*, 3339-3346.
- [77] TINKER V7.1-2015, Software tools for molecular design, Jay Ponder Lab, Department of Chemistry, Washington University, Saint Louis, Missouri 63130 U.S.A.; available from <http://dasher.wustl.edu/tinker/>
- [78] A. Klamt, G. Schüürmann *J. Chem. Soc., Perkin Trans. 2* **1993**, 799-805.
- [79] TURBOMOLE V7.1, University of Karlsruhe and Forschungszentrum Karlsruhe GmbH, 1989-2007, TURBOMOLE GmbH; 2015; <https://www.turbomole.org>

Entry for the Table of Contents



ATR-FTIR spectra of acetate alkali-metal solutions display a cation-dependent behavior which can be correlated to ion pair formation. Simulations in explicit solvent and frequency calculations are used to identify the main supramolecular structures present in solution.

Keywords

Density functional calculations; Ion pairs; IR spectroscopy; Structure elucidation;